Ajaj, R. M., Omar, F. K., Darabseh, T. T., & Cooper, J. (2019). Flutter of Telescopic Span Morphing Wings. *International Journal of Structural Stability and Dynamics*, *19*(6), [1950061]. https://doi.org/10.1142/S0219455419500615

International Journal of Structural Stability and Dynamics
Vol. 19, No. 6 (2019) 1950061 (24 pages)

DOI: 10.1142/S0219455419500615

Flutter of Telescopic Span Morphing Wings

Rafic M. Ajaj*,§, Farag K. Omar*, Tariq T. Darabseh*,‡ and Jonathan Cooper†

*Department of Mechanical Engineering
United Arab Emirates University, Al Ain, UAE

†Department of Aerospace Engineering
Dynamics and Control Group, University of Bristol
Bristol BS8 1TR, UK

‡Department of Aeronautical Engineering
Jordan University of Science and Technology, Irbid, Jordan
§raficajaj@uaeu.ac.ae

Received 16 August 2018
Accepted 11 February 2019
Published 3 May 2019

This paper studies the aeroelastic behavior of telescopic, multi-segment, span morphing wings. The wing is modeled as a linear, multi-segment, stepped, cantilever Euler–Bernoulli beam. It consists of three segments along the axis and each segment has different geometric, mechanical, and inertial properties. The aeroelastic analysis takes into account spanwise out-of-plane bending and torsion only, for which the corresponding shape functions are derived and validated. The use of shape functions allows representing the wing as an equivalent aerofoil whose generalized coordinates are defined at the wingtip according to the Rayleigh–Ritz method. Theodorsen's unsteady aerodynamic theory is used to estimate the aerodynamic loads. A representative Padé approximation for the Theodorsen's transfer function is utilized to model the aerodynamic behaviors in state-space form allowing time-domain simulation and analysis. The effect of the segments' mechanical, geometric, and inertial properties on the aeroelastic behavior of the wing is assessed. Finally, the viability of span morphing as a flutter suppression device is studied.

Keywords: Telescopic wing; span morphing; flutter; aeroelasticity.

Nomenclature

$\hat{a}$ = normalized pitch axis location with respect to half chord
($\hat{a} = -1$ leading edge, $\hat{a} = 1$ trailing edge)
b = wingspan

§Corresponding author.

c = chord of the aerofoil/wing
$\bar{E}I$ = bending rigidity
$\bar{G}J$ = torsional rigidity
$h(y)$ = bending shape function
I'_{ea} = mass moment of inertia around the elastic axis
l = length
L' = lift per unit span
L = equivalent lift force
LE = leading edge
m' = mass per unit span
M'_{ea} = pitching moment per unit span around the elastic axis
M_{ea} = equivalent pitching moment around the elastic axis
s = Laplace variable
t = time
T = total kinetic energy
U = total potential energy
V = true airspeed
x_θ = distance between elastic axis and center of gravity
w = plunge displacement at elastic axis
y = spanwise location measured relative to the wing root
θ = pitch angle
$\phi(y)$ = torsion shape function
ρ = air density

Subscripts

t = wingtip
1 = Segment 1
2 = Segment 2
3 = Segment 3
i = ith vibration mode
j = jth wing segment

Superscripts

$.$ = first time derivative
$..$ = second time derivative
$,$ = first spatial derivative
$,,$ = second spatial derivative

1. Introduction

A large wingspan/aspect ratio improves the aerodynamic efficiency but reduces maneuvrability, whereas a small wingspan improves maneuvrability but reduces aerodynamic efficiency.[1] The span morphing technology allows integrating the benefits of both large wingspan and small wingspan into one aircraft to effectively perform a wide range of missions.[2–4] Ajaj *et al.*[3,4] studied the benefits of variable span wings to enhance the aerodynamic efficiency when actuated symmetrically and to improve roll control when actuated asymmetrically. Span morphing wings have been developed since the start of powered flight. For instance, the MAK-10 aircraft, develop by Ivan Makhonine, flew in the 1930s with a telescopic span morphing wing. Makhonine utilized pneumatic actuators to move the telescopic wing to achieve span extensions up to 60%.[5] Recently, there has been some promising work on telescopic span morphing wings. For example, Blondeau and Pines[6] developed a telescopic wing where hollow shells were used to preserve the aerofoil shape and reduce the storage size of the wing. They utilized inflatable actuators to withstand the different loads on the wing. Bae *et al.*[7] studied wings of a long-range cruise missile and highlighted some of the main challenges associated with the design of a span morphing wing. They achieved drag reduction of 25% and a range increase of 30%. Ajaj and Jankee[8] developed the Transformer Aircraft, a span morphing UAV, capable of symmetric and asymmetric span extensions. A novel actuation system based on a rack and pinion mechanism was utilized. They conducted extensive wind tunnel and flight testing to assess the effect of span morphing on the flight mechanics and aerodynamic efficiency.

Similarly, Santos *et al.*,[9] Mestrinho *et al.*,[10] and Felício *et al.*[11] and developed and tested a variable-span morphing wing (VSW) to be fitted on a mini-UAV. They achieved 20% wing drag reduction with symmetric span extension. The roll rate achieved with asymmetric span morphing matched the aileron in terms of roll power. The VSW was constructed from composite materials and was actuated using an electro-mechanical mechanism. Mechanical testing was performed to evaluate the behavior of the wing under various loading scenarios. Flight testing showed full functionality of the VSW and its aerodynamic improvements compared with conventional fixed wing. A more extensive review on span morphing wings (applications and concepts) for both fixed-wing and rotary-wing aircraft is given in Barbarino *et al.*[1]

Recently, there have been a number of attempts to study the aeroelastic behavior of span morphing wings. For example, Ajaj and Friswell[12] developed a linear, time-domain aeroelastic model that uses Theodorsen's unsteady aerodynamics to study the aeroelastic behavior of compliant span morphing wings. They performed extensive sensitivity studies and concluded that span morphing can be used as an effective flutter suppression device. Similarly, Huang and Qiu[13] developed a novel first-order state-space aeroelastic model based on Euler–Bernoulli beam theory. They assumed time-dependent boundary conditions coupled with a reduced-order

unsteady vortex lattice method. Similarly, Li and Jin[14] studied the dynamical behavior and stability of a variable-span wing subjected to supersonic aerodynamic loads. They modeled the span morphing wing as an axially moving cantilever plate and established the governing equations of motion using Kane's method and piston theory. They concluded that a periodically varying (with proper amplitude) morphing law can facilitate flutter suppression. Gamboa *et al.*[15] studied the aeroelasticity of composite VSW intended for a small UAV. The study concentrated on the flutter critical speed estimation and assessed the effect of the interface between fixed and moving wing parts. Their aerodynamic solver was based on an unsteady linearized potential theory coupled with three-dimensional lifting surface strip theory approximation for lifting surfaces with high aspect ratio. The results showed that the wing can fly safely within the intended speed envelope.

The aim of this paper is to investigate the aeroelastic behavior of telescopic span morphing wings. The wing is modeled as a stepped, multi-segment Euler–Bernoulli beam consisting of three main segments with different geometric, inertial, and mechanical properties. Theodorsen's aerodynamic theory is utilized for estimating the unsteady aerodynamic loads. The influence of the segments' properties on the binary (bending-torsion) aeroelastic behavior of the wing is assessed. Goland wing[16] and the HALE wing[17] are used as the basis of this study. The effect of the segments properties on the flutter mode is investigated. Finally, the feasibility of utilizing span morphing as an active flutter suppression device is assessed.

2. Aeroelasticity Model

The wing is modeled as a stepped Euler–Bernoulli beam consisting of three segments. These segments correspond to the fixed wing partition, the overlapping region, and the extending partition as shown in Fig. 1.

Across each segment, the mechanical and geometric properties are uniform but they differ from one segment to another. The properties (considered here) corresponding to each segment are listed in Table 1. Each segment is rectangular,

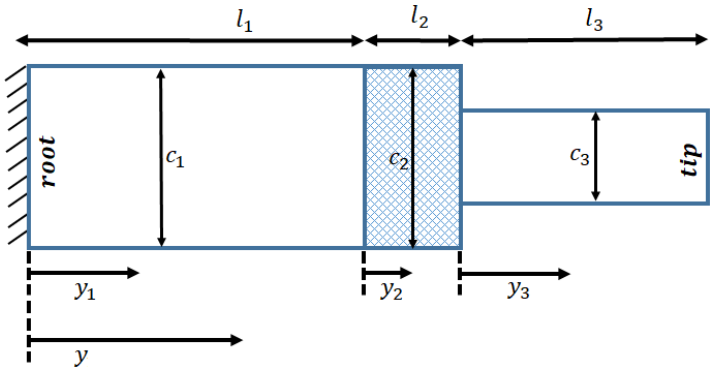

Fig. 1. A top view of the telescopic span morphing wing.

Table 1. Geometric and mechanical properties of the multi-segment wing.

Parameter	Segment 1	Segment 2	Segment 3
Bending rigidity	$(EI)_1$	$(EI)_2$	$(EI)_3$
Torsional rigidity	$(GJ)_1$	$(GJ)_2$	$(GJ)_3$
Length	l_1	l_2	l_3
Chord	c_1	c_2	c_3
Mass per unit span	m'_1	m'_2	m'_3
Mass moment of inertia per unit span	I'_{ea_1}	I'_{ea_2}	I'_{ea_3}
CG location from LE	x_{cg_1}	x_{cg_2}	x_{cg_3}
EA location from LE	x_{ea_1}	x_{ea_2}	x_{ea_3}
Distance between EA and CG	x_{θ_1}	x_{θ_2}	x_{θ_3}
Spanwise position	$0 \le y_1 \le l_1$	$0 \le y_2 \le l_2$	$0 \le y_3 \le l_3$

unswept, untapered to minimize geometric and aeroelastic couplings. It is assumed to have a clean wing configuration where no control surfaces or engines are attached to it, and there are no fuel tanks embedded within. The continuous, multi-degree-of-freedom wing structure is modeled as a two-degree-of-freedom system via the Rayleigh–Ritz method using bending and torsion shape functions. These shape functions correspond to the uncoupled first bending and first torsional modes of a stepped cantilever beam. This allows the wing to be modeled as an equivalent two-degree-of-freedom aerofoil whose generalized coordinates are defined at the wingtip. The dynamics of the telescopic mechanism are neglected (as the rate of span extension or retraction is low). Using the shape functions, the plunge displacement, speed, and acceleration at any spanwise location (y) and time instant can now be related to those of the wingtip (generalized coordinates) as:

$$\begin{aligned} w(t,y) &= w_t(t)h(y), \\ \dot{w}(t,y) &= \dot{w}_t(t)h(y), \\ \ddot{w}(t,y) &= \ddot{w}_t(t)h(y). \end{aligned} \tag{1}$$

Similarly, the pitch displacement, speed, and acceleration at any spanwise location (y) and time instant can now be related to those of the wingtip (generalized coordinates) as

$$\begin{aligned} \theta(t,y) &= \theta_t(t)\phi(y), \\ \dot{\theta}(t,y) &= \dot{\theta_t}(t)\phi(y), \\ \ddot{\theta}(t,y) &= \ddot{\theta_t}(t)\phi(y), \end{aligned} \tag{2}$$

where $w_t(t)$ and $\theta_t(t)$ represent the generalized coordinates coinciding with the wingtip. It should be noted that the datum from which the generalized coordinates are measured is the static position of the wingtip when the wing deflects under self-weight.

2.1. *Bending shape functions*

To obtain the bending shape functions, the continuity and boundary conditions listed in Table 2 are considered.

Table 2. Bending boundary conditions.

Root conditions	Continuity conditions	Tip conditions
$w_1(t, y_1 = 0) = 0$	$w_1(t, y_1 = l_1) = w_2(t, y_2 = 0)$	$\frac{\partial^2 w_3(t, y_3 = l_3)}{\partial y_3^2} = 0$
$\frac{\partial w_1(t, y_1 = 0)}{\partial y_1} = 0$	$\frac{\partial w_1(t, y_1 = l_1)}{\partial y_1} = \frac{\partial w_2(t, y_2 = 0)}{\partial y_2}$	$\frac{\partial^3 w_3(t, y_2 = l_3)}{\partial y_3^3} = 0$
	$(EI)_1 \frac{\partial^2 w_1(t, y_1 = l_1)}{\partial y_1^2} = (EI)_2 \frac{\partial^2 w_2(t, y_2 = 0)}{\partial y_2^2}$	
	$(EI)_1 \frac{\partial^3 w_1(t, y_1 = l_1)}{\partial y_1^3} = (EI)_2 \frac{\partial^3 w_2(t, y_2 = 0)}{\partial y_2^3}$	
	$w_2(t, y_2 = l_2) = w_3(t, y_2 = 0)$	
	$\frac{\partial w_2(t, y_2 = l_2)}{\partial y_2} = \frac{\partial w_3(t, y_3 = 0)}{\partial y_3}$	
	$(EI)_2 \frac{\partial^2 w_2(t, y_2 = l_2)}{\partial y_2^2} = (EI)_3 \frac{\partial^2 w_3(t, y_3 = 0)}{\partial y_3^2}$	
	$(EI)_2 \frac{\partial^3 w_2(t, y_2 = l_2)}{\partial y_2^3} = (EI)_3 \frac{\partial^3 w_3(t, y_3 = 0)}{\partial y_3^3}$	

The bending shape function, $h_i(y)$, corresponding to the ith bending mode is given as:

$$h_i(y) = \begin{cases} h_{1_i}(y) & 0 \le y \le l_1 \\ h_{2_i}(y) & l_1 < y \le l_1 + l_2 \\ h_{3_i}(y) & l_1 + l_2 < y \le l_1 + l_2 + l_3 \end{cases}. \tag{3}$$

Appendix A details the steps to obtain the bending shape function and natural frequency corresponding to the ith mode.

2.2. *Torsion shape functions*

Similarly, to obtain the torsion shape function, the boundary and continuity conditions listed in Table 3 are considered.

The torsion shape function $\phi_i(y)$ corresponding to the ith torsional vibration mode is given as:

$$\phi_i(y) = \begin{cases} \phi_{1_i}(y) & 0 \le y \le l_1 \\ \phi_{2_i}(y) & l_1 < y \le l_1 + l_2 \\ \phi_{3_i}(y) & l_1 + l_2 < y \le l_1 + l_2 + l_3 \end{cases}. \tag{4}$$

Table 3. Torsion boundary conditions.

Root conditions	Continuity conditions	Tip conditions
$\theta_1(t, y_1 = 0) = 0$	$\theta_1(t, y_1 = l_1) = \theta_2(t, y_2 = 0)$	$\frac{\partial \theta_3(t, y_3 = l_3)}{\partial y_3} = 0$
	$(GJ)_1 \frac{\partial \theta_1(t, y_1 = l_1)}{\partial y_1} = (GJ)_2 \frac{\partial \theta_2(t, y_2 = 0)}{\partial y_2}$	
	$\theta_2(t, y_2 = l_2) = \theta_3(t, y_3 = 0)$	
	$(GJ)_2 \frac{\partial \theta_2(t, y_2 = l_2)}{\partial y_2} = (GJ)_3 \frac{\partial \theta_3(t, y_3 = 0)}{\partial y_3}$	

Appendix B details the steps to obtain the torsion shape function and natural frequency corresponding to the ith mode.

2.3. *Equations of motion*

The total kinetic energy (T) and total potential energy (U) of the three segments' cantilever, rectangular wing can be expressed as

$$\begin{aligned} T = {} & \frac{1}{2}\dot{w}_t^2\left(\int_0^{l_1} m_1' h_1^2 dy + \int_{l_1}^{l_2} m_2' h_2^2 dy + \int_{l_2}^{l_3} m_3' h_3^2 dy\right) \\ & + \frac{1}{2}\dot{\theta}_t^2\left(\int_0^{l_1} I_{\mathrm{ea}_1}' \phi_1^2 dy + \int_{l_1}^{l_2} I_{\mathrm{ea}_2}' \phi_2^2 dy + \int_{l_2}^{l_3} I_{\mathrm{ea}_3}' \phi_3^2 dy\right) \\ & - \dot{w}_t\dot{\theta}_t\left(\int_0^{l_1} m_1' x_{\theta_1} h_1 \phi_1 dy + \int_{l_1}^{l_2} m_2' x_{\theta_2} h_2 \phi_2 dy + \int_{l_2}^{l_3} m_3' x_{\theta_3} h_3 \phi_3 dy\right) \end{aligned} \tag{5}$$

and

$$\begin{aligned} U = {} & \frac{1}{2}\theta_t^2\left(\int_0^{l_1} (GJ)_1\left(\frac{d\phi_1}{dy}\right)^2 dy + \int_{l_1}^{l_2} (GJ)_2\left(\frac{d\phi_2}{dy}\right)^2 dy + \int_{l_2}^{l_3} (GJ)_3\left(\frac{d\phi_3}{dy}\right)^2 dy\right) \\ & + \frac{1}{2}w_t^2\left(\int_0^{l_1} (EI)_1\left(\frac{d^2h_1}{dy^2}\right)^2 dy + \int_{l_1}^{l_2} (EI)_2\left(\frac{d^2h_2}{dy^2}\right)^2 dy + \int_{l_2}^{l_3} (EI)_3\left(\frac{d^2h_3}{dy^2}\right)^2 dy\right). \end{aligned} \tag{6}$$

It should be noted that structural damping is not considered in this study; this assumption is commonplace in aeroelastic analysis as any structural damping will increase the speed at which flutter will occur. Using the expressions of kinetic and potential energies, the full equations of motion of the span morphing wing can developed using Lagrangian mechanics as:

$$\frac{d}{dt}\left(\frac{\partial(T-U)}{\partial \dot{w}_t}\right) - \frac{\partial(T-U)}{\partial w_t} = L, \tag{7}$$

$$\frac{d}{dt}\left(\frac{\partial(T-U)}{\partial \dot{\theta}_t}\right) - \frac{\partial(T-U)}{\partial \theta_t} = M_{\mathrm{ea}}, \tag{8}$$

where L is the generalized lift force and M_{ea} is the generalized pitching moment. The generalized lift force and pitching moment around the elastic axis can be obtained as:

$$L = \int_0^{l_1} L_1' h_1(y) dy + \int_{l_1}^{l_2} L_2' h_2(y) dy + \int_{l_2}^{l_3} L_3' h_3(y) dy \tag{9}$$

and

$$M_{\mathrm{ea}} = \int_0^{l_1} M_{\mathrm{ea}_1}' \phi_1(y) dy + \int_{l_1}^{l_2} M_{\mathrm{ea}_2}' \phi_2(y) dy + \int_{l_2}^{l_3} M_{\mathrm{ea}_2}' \phi_3(y) dy, \tag{10}$$

where L'_1, L'_2, and L'_3 are the unsteady lift per unit span on segments 1, 2, and 3, respectively. M'_{ea_1}, M'_{ea_2}, and M'_{ea_3} are the unsteady pitching moments around the elastic axis per unit span on segments 1, 2, and 3, respectively. It should be noted that the expression of lift per unit span and pitching moment per unit span will vary for the different segments due to different chords and different distances between aerodynamic centers and elastic axis of each segment.

2.4. *Aerodynamics*

The aerodynamic loads acting on the wing are modeled according to Theodorsen's unsteady aerodynamics theory. Theodorsen's unsteady aerodynamic model consists of a circulatory component accounting for the effect of the wake on the aerofoil (contains the main aerodynamic damping and aerodynamic stiffness terms) and a noncirculatory component accounting for the acceleration of the fluid surrounding the aerofoil.[18] The work of Theodorsen is based on the following assumptions:

- Thin aerofoil;
- Potential, incompressible flow;
- The flow remains attached, i.e. the amplitude of oscillations is small and the wake behind the aerofoil is flat.

According to Theodorsen's unsteady aerodynamic theory, L'_j and M'_{ea_j}, acting on the jth wing segment can be expressed, respectively, as

$$L'_j = \pi\rho\frac{c_j^2}{4}\left[-\ddot{w} + V\dot{\theta} - \frac{\hat{a}_j c_j}{2}\ddot{\theta}\right] + 2\pi\rho V\frac{c_j}{2}C(k)\left[-\dot{w} + V\theta + \frac{c_j}{2}\left(\frac{1}{2} - \hat{a}_j\right)\dot{\theta}\right] \quad (11)$$

and

$$M'_{\mathrm{ea}_j} = L'_j\left[\frac{c_j}{4} + \frac{\hat{a}_j c_j}{2}\right] + \pi\rho\frac{c_j^3}{8}\left[\frac{\ddot{w}}{2} - V\dot{\theta} - \frac{c_j}{2}\left(\frac{1}{8} - \frac{\hat{a}_j}{2}\right)\ddot{\theta}\right], \quad (12)$$

where ρ is the air density, c_j is the chord of the wing at any jth segment, and $\hat{a}_j = \frac{2x_{\mathrm{ea}_j}}{c_j} - 1$ is the normalized pitch axis location with respect to half chord of the jth segment. $C(k)$ is the frequency-dependent, Theodorsen's transfer function that accounts for attenuation of lift amplitude and phase lag in lift response due to sinusoidal motion. In this paper, unsteady lift per unit span and pitching moment per unit span are expressed in time domain. Therefore, a Padé approximation for Theodorsen's transfer function was used.[20,21] The approximate transfer function $C(s)$ in the Laplace domain becomes

$$C(s) \approx \frac{0.5177a_j^2 s^2 + 0.2752a_j s + 0.01576}{a_j^2 s^2 + 0.3414a_j s + 0.01582}, \quad (13)$$

where

$$a_j = \frac{c_j}{2V}. \quad (14)$$

The Padé approximation for Theodorsen function is highly accurate especially at low reduced frequencies which is the case in this paper. For more details on the expression of unsteady lift and moment in state-space form, the reader is advised to consult Ajaj and Friswell.[12] A similar analysis was performed by Duan and Zhang[19] in which they used Fourier transform to formulate the aeroelastic equations of motion of a wing in a state-space form.

2.5. *Validation*

The aeroelastic model is validated using Goland wing and HALE wing whose mechanical and geometric properties are listed in Table 4. The wings studied here are of high aspect ratio to be consistent with the Euler–Bernoulli formulation (ignoring the shear deformation of the wing cross-section).

The flutter speed, frequency, and divergence speed estimated for the Goland and HALE wings are presented in Table 5. Table 5 shows a comparison with estimates from various other methods available in literatures.

Table 4. Geometric and mechanical properties of Goland and HALE wings.

Specifications	Goland wing	HALE wing
Half span (m)	6.096	16
Chord (m)	1.8288	1
Mass per unit length (kg/m)	35.71	0.75
Moment of inertia (50% chord) (kg m)	8.64	0.1
Spanwise elastic axis (from LE)	33%	50%
Center of gravity (from LE)	43%	50%
Spanwise bending rigidity (Nm^2)	9.77×10^6	2×10^4
Torsional rigidity ($N\ m^2$)	0.987×10^6	1×10^4
Chordwise bending rigidity ($N\ m^2$)	—	4×10^6
Density of air (kg/m^3)	1.225	0.0889

Table 5. Validation using Goland and the HALE wings.

	Method						
	Present work (binary)	Present work (eight modes)	Ref. 22	Ref. 23	Ref. 17	Ref. 24	Ref. 14
HALE wing							
Flutter speed (m/s)	33.43	33.00	32.21	—	—	32.51	—
Flutter freq. (rad/s)	21.38	21.75	22.61	—	—	22.37	—
Divergence speed (m/s)	37.18	37.20	37.29	—	—	37.15	—
Goland wing							
Flutter speed (m/s)	137.11	137.01	—	135.6	136.22	137.16	133
Flutter freq. (rad/s)	69.9	69.93	—	70.2	70.06	70.7	72.7
Divergence speed (m/s)	252.8	252.97	—	—	250.82	—	—

2.6. *Variation of the uncoupled shape functions with wing properties (aerodynamics OFF)*

In this section, it is assumed that Goland wing is extended by 50% so that the wing semi-span is 9.144 m. The wing consists of three main segments. Segment 1 represents the main wing (without overlapping region), whereas Segment 2 represents the overlapping region and Segment 3 represents the extension. The mechanical and geometric properties of Segment 1 are exactly the same as those of Goland wing (listed in Table 3) except the length of Segment 1 is $l_1 = 5$ m. Segment 2 has a length $l_2 = 1.096$ m, whereas Segment 3 has a length $l_3 = 3.048$ m. Two scenarios are studied here, and in both scenarios it is assumed that the locus of the center of gravity (CG) of the three segments is a continuous line starting at the wing root and ending at its tip. Similarly, the locus of the shear center of the three segments is a continuous line starting at the wing root and ending at its tip. The Transformer Aircraft[8] is a good example where the loci of the CG and shear entre are continuous straight lines.

i. *Scenario* 1

In Scenario 1, Segments 1 and 2 are assumed to have the same chords, bending rigidity, and torsional rigidity. The properties of Segment 3 are varied, and the bending and torsion shape functions for the first bending and torsion modes associated with changes in Segment 3 chord are presented in Figs. 2(a) and 2(b). The chord of Segment 3 is varied as a fraction of the Segment 1 chord. A change in the chord of Segment 3 results in changes in the bending rigidity, torsion rigidity, mass per unit span, inertia per unit span according to the expressions in Table 6.

ii. *Scenario* 2

In Scenario 2, Segments 1 and 3 are assumed to have the same mechanical and inertial properties. The chord of Segment 2 is varied as fraction of the chord of Segment 1. The properties of Segment 2 vary according to the expressions listed in Table 6. The variations of the uncoupled first bending and first torsion shape functions with Segment 2 chord are shown in Figs. 2(c) and 2(d).

It can be seen from Figs. 2(a) and 2(c) that as the bending stiffness of Segment 3 or of Segment 2 reduces, the contribution of Segment 1 to the mode shape will be much smaller than the contributions of Segments 2 and 3. On the contrary, the first torsional mode shape is more sensitive to variations in properties (mainly torsional rigidity) of Segment 2 than of Segment 3. This can be clearly noticed when comparing Figs. 2(b) and 2(d). Large variations in the torsional rigidity of Segment 2 severely distort the first torsion mode shape. Depending on the length of Segment 2, this can significantly affect the aeroelastic stability of the wing.

Figure 3 shows the variation of the uncoupled first bending and first torsion natural frequencies for each scenario. Increasing the chord of Segment 3

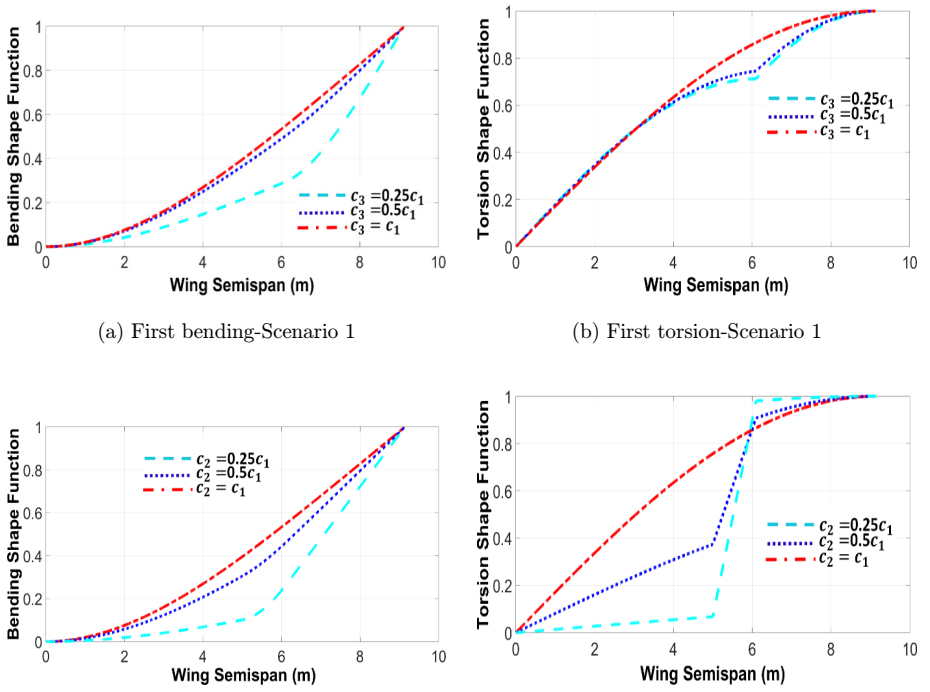

(a) First bending-Scenario 1

(b) First torsion-Scenario 1

(c) First bending-Scenario 2

(d) First torsion-Scenario 2

Fig. 2. Variation of first bending and first torsion shape functions.

Table 6. Correlations between Segments 1 and 3.

$(GJ)_3 = (GJ)_1\left(\frac{c_3}{c_1}\right)^3$	$m'_3 = m'_1\left(\frac{c_3}{c_1}\right)$
$(EI)_3 = (EI)_1\left(\frac{c_3}{c_1}\right)^3$	$I'_{\text{ea}_3} = I'_{\text{ea}_1}\left(\frac{c_3}{c_1}\right)^3$

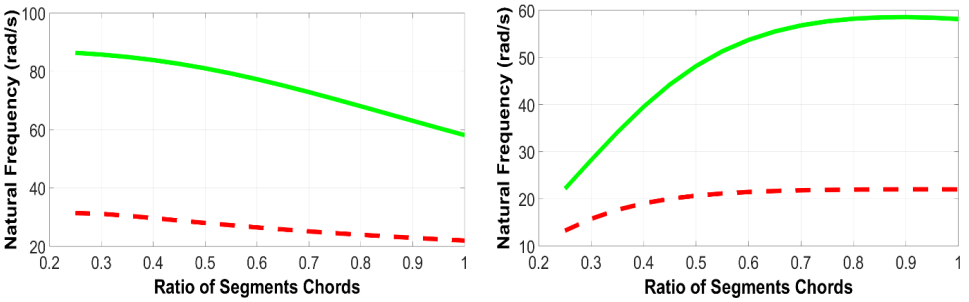

(a) Scenario 1

(b) Scenario 2

Fig. 3. Variation of first bending and first torsion natural frequencies (solid line is for torsion and dashed line is for bending).

(while keeping the properties of the other segments constant) reduces the bending and torsion natural frequencies. On the contrary, increasing the chord of Segment 2 (while keeping the properties of the other segments constant) increases the first bending and first torsion natural frequencies. It can be noticed that the change in the natural frequencies is negligible when the chord of Segment 2 is above 75% of chord of Segment 1.

3. Quasi-Static Aeroelastic Study: Binary Flutter

3.1. *Effect of Segment 3 on flutter*

In this section, the wingspan is extended quasi-statically to determine the effect of span extension on the flutter speed, frequency, and divergence speed. The HALE wing, whose properties are listed in Table 4, is used as the basis for this study. The properties of Segment 3 are varied to assess the effect of its mechanical, inertial, and geometric properties on the flutter speed. Two wing models are used in this study. The first is a two-segment model in which the wing consists of two segments (Segments 1 and 3) and the overlapping region is not considered. The second is a three-segment model in which the wing consists of three segments: Segments 1, 2, and 3. Segment 2 represents the overlapping section whose length varies as the wingspan extends. In the three-segment model, the properties of Segment 2 (overlapping region) such as mass per unit span, torsional, and bending rigidity depend on those of Segments 1 and 3. Figure 4 shows the variation of the aeroelastic behavior of the multi-segment span morphing wing for different configurations of Segment's 3. It should be noted that in Fig. 4 the flutter speed, frequency, and divergence speed are normalized by the corresponding values associated with the baseline (nonmorphing) Hale wing (listed in Table 5). Three different configurations of Segment 3 are studied here. They correspond to the chord of Segment 3 being equal to 40%, 70%, and 100% of Segment's 1 chord. For each configuration of Segment 3, its properties change according to the relationships expressed in Table 6.

It can be seen that for a given span extension, configurations with smaller chords (of Segment 3) have higher flutter speed and frequency. This is true for both models (two-segments and three-segments). In general, span extension results in reduction in flutter speed, which reduces the flight envelope of the aircraft. As the chord of Segment 3 (and the associated properties) gets smaller, the sensitivity of flutter and divergence speeds with span extension reduce significantly. It can be seen from Fig. 4(b) that when the chord of Segment 3 is the same as the chord of Segment 1, increasing the wingspan by 50% reduces the flutter speed by 35%. In contrast, when the chord of Segment 3 is 40% of the chord of Segment 1, the flutter speed reduces by 10% at 50% span extension.

The results from the two different models show the influence of the overlapping region on the aeroelastic behavior. In Figs. 4(b), 4(d), and 4(f), the normalized

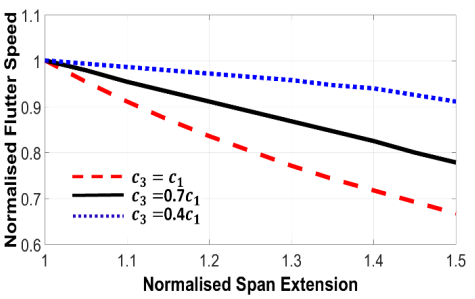

(a) Flutter speed (2 Segments model)

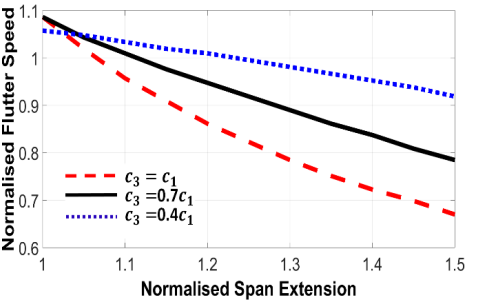

(b) Flutter speed (3 Segments model)

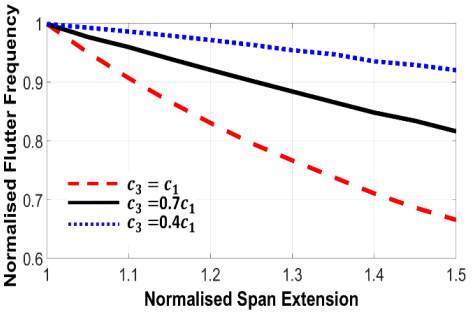

(c) Flutter frequency (2 Segments model)

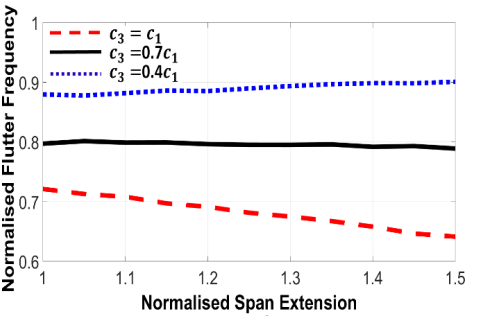

(d) Flutter frequency (3 Segments model)

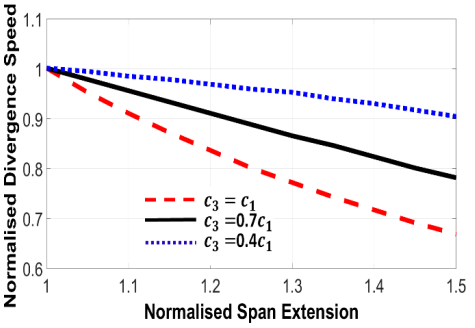

(e) Divergence speed (2 Segments model)

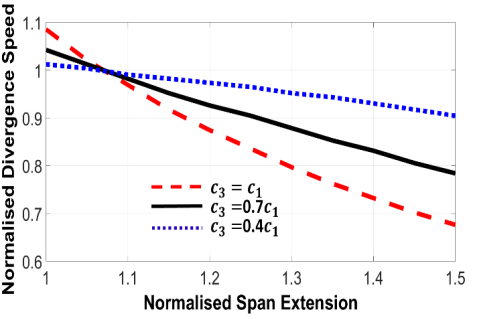

(f) Divergence speed (3 Segments model)

Fig. 4. Aeroelastic behavior of the extended wing versus Segment's 3 properties.

flutter speed, divergence speed, and frequency do not start from unity as with the two-segment model. As the wingspan increases, the length of Segment 2 reduces and hence its influence on the aeroelastic behavior of the wing. It should be noted that the three-segment model treats the overlapping region as an idealized joint and does not take into account any form of localized stiffness, damping, and/or freeplay that may

exist in real telescopic joints. As the wingspan extends by 50%, the length of the overlapping segment shrinks to become 10% of the baseline semi-span (16 m). Figure 4(b) shows that at zero span extension, the flutter speed is higher than that of the uniform baseline wing (nonmorphing) by around 8%.

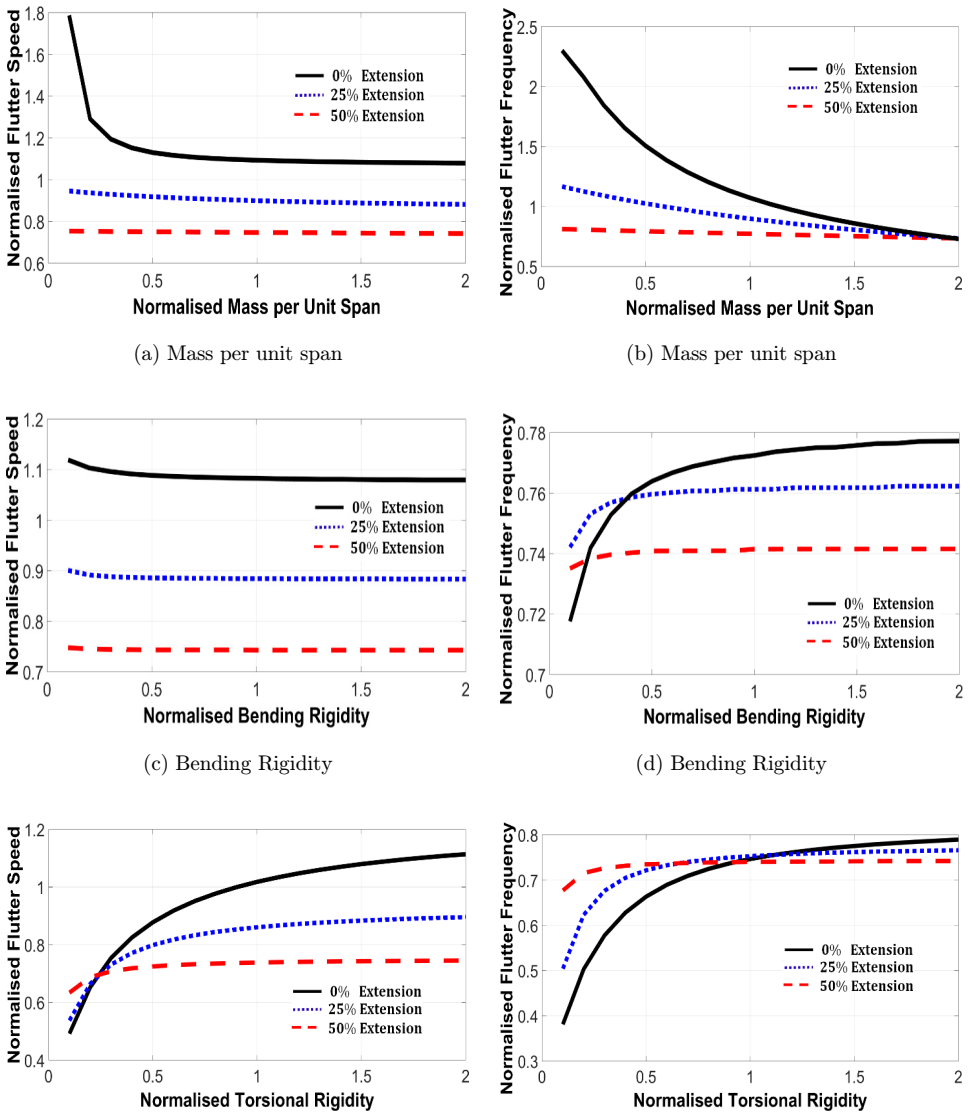

(a) Mass per unit span

(b) Mass per unit span

(c) Bending Rigidity

(d) Bending Rigidity

(e) Torsional Rigidity

(f) Torsional Rigidity

Fig. 5. Influence of the overlapping segment on the aeroelastic behavior of the Hale wing.

3.2. *Effect of overlapping segment on flutter*

It is essential to assess the effect of the overlapping segment (Segment 2) on the aeroelastic behavior of the wing. Three main parameters of Segment 2, including mass per unit span, bending rigidity, and torsional rigidity, are studied at different wingspans (corresponding to 0%, 25%, and 50% extensions). The chord of Segment 3 is set at 80% of the chord of Segment 1. During this sensitivity study, only one parameter is varied at a time. For instance, when the torsional rigidity of Segment 2 varies between 0.1 and 2 times the torsional rigidity of Segment 1, the bending rigidity and mass per unit span of Segment 2 are kept constants.

It can be seen that regardless of the parameter investigated, the sensitivity of flutter speed and frequency reduce as the wingspan is extended and the size of the overlapping region drops. However, when the HALE wing is fully retracted, the effect of Segment 2 parameters on the aeroelastic behavior of the wing is significant. It can be seen from Fig. 5 that flutter is most sensitive to torsional rigidity followed by the mass per unit span. The bending rigidity of Segment 2 has minor effect on flutter speed and frequency, irrespective of the span extension. It can also be seen that when the wing is fully retracted (and the length of Segment 2 is maximum), the flutter speed and frequency are very sensitive to mass per unit span especially when the ratio of the mass of Segment 2 to mass of Segment 1 is less than 0.5. It should be noted that it is impractical to have the ratio of the masses less than 1 at least for wing studied here.

4. Multimode Flutter Analysis

Section 3 of this paper focussed on the effect of the segment properties on the binary (bending-torsion) aeroelastic behavior of the wing. However, it is essential to determine the effect of span morphing on the flutter mode. Therefore, the three-segment binary aeroelastic model (discussed in Sec. 3) is extended to include high-order vibration modes, mainly the first, second, third, and fourth bending modes and the first, second, third, and fourth torsion modes. For the baseline (nonmorphing) Goland and HALE wings, the flutter speed and flutter frequency and divergence speed obtained using the multimode aeroelastic model are listed in Table 5. Goland wing is used as the baseline wing in this section. The variation of the different modes with airspeed for the baseline (nonmorphing) Goland wing and for the telescopic span morphing Goland wing at 50% extension is shown in Fig. 6. For the results in Fig. 6, the chord of Segment 3 (extension) is set equal to the chord of Segment 1.

The morphing wing at 50% span extension flutters at around 100 m/s compared with 137 m/s for the nonmorphing baseline Goland wing. It should be noted that the modal damping of the first bending mode (mode 1) increases with airspeed at a higher rate for the extended morphing wing compared with the baseline wing. The same is true for the first torsion mode in which the modal damping initially increases at a higher rate; then once a critical speed is reached, it reduces at a higher rate when

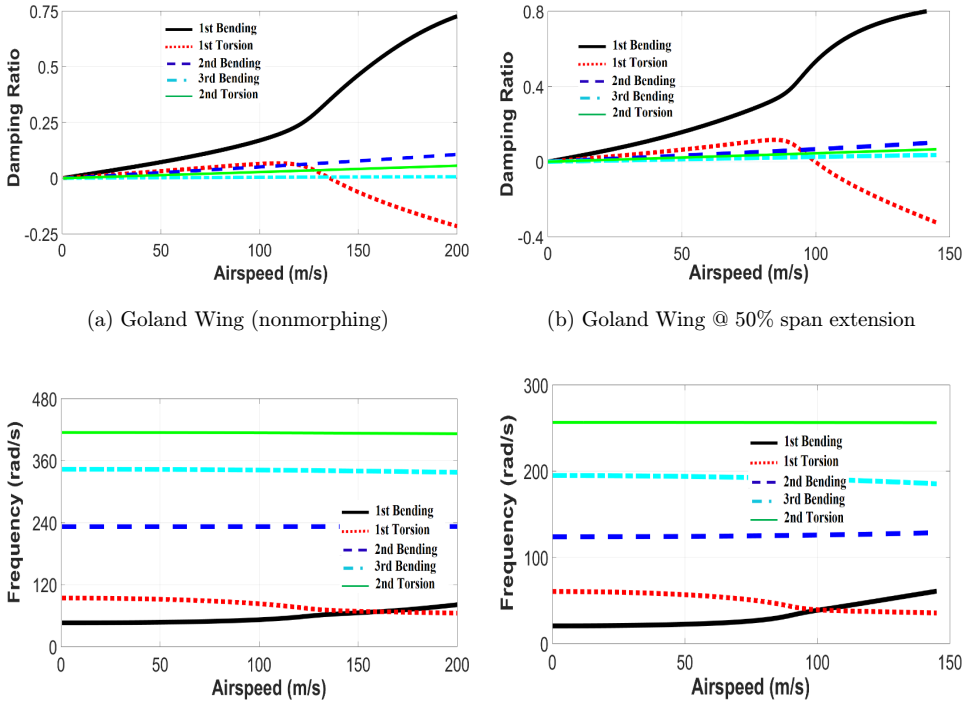

(a) Goland Wing (nonmorphing)

(b) Goland Wing @ 50% span extension

(c) Goland Wing (nonmorphing)

(d) Goland Wing @ 50% span extension

Fig. 6. Frequency and damping trends for the Goland wing at different span extensions.

compared with the baseline nonmorphing wing. Figure 6 shows that span extension does not change the flutter mode for the clean rectangular wing considered here (without engines, control surfaces, and fuel tanks). For both the morphing wing and the nonmorphing, the first torsion mode (mode 2) is the first to go unstable.

5. Flutter Suppression

The aim of this section is to assess the feasibility of using span morphing as an effective flutter suppression device. Two main scenarios are studied to demonstrate the flutter suppression capability. A telescopic span morphing wing whose baseline dimensions (before span extension) are similar to those of the Goland wing is considered. Different flight conditions are used to assess the viability of the device at a range of operating conditions.

i. *Scenario* 1: *Span retraction at flutter speed*

The telescopic span morphing Goland wing is set at 5° angle of attack with an airspeed equal to the flutter speed at 25% span extension. Once released into the airflow, the wing starts a series of undamped oscillations in pitch and plunge. At

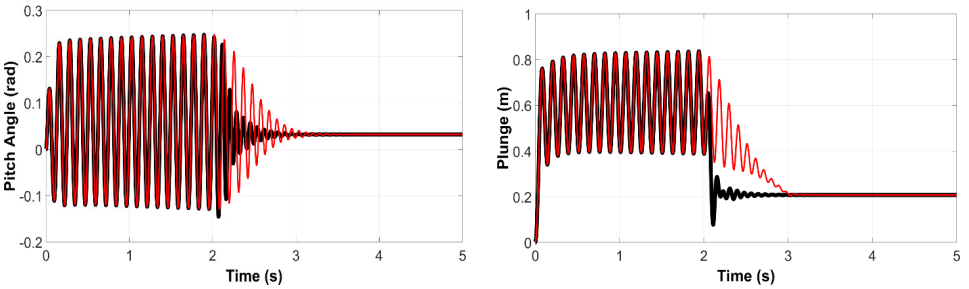

(a) Wingtip pitch angle (b) Wingtip plunge

Fig. 7. (Color online) Goland wing at the flutter speed and 5° AOA. At $t = 2$ s, the semi-span is retracted by 25%. Two retraction speeds are considered (red thin curve for 1.5240 m/s and black thick curve for 15.240 m/s).

$t = 2$ s, the wingspan is retracted by 25% (new wing semi-span is 6.096 m). Two retraction speeds are studied (1.5240 m/s and 15.240 m/s). The behavior of the wing for the different retraction speeds can be seen in Fig. 7. Figure 7 shows that span retraction damps the oscillations in pitch and plunge. As the span retraction rate increases, the wing oscillations decay faster. This is mainly due to the fact that as the wingspan is reduced, its bending and torsional stiffness increases, resulting in an increase in the flutter speed.

ii. *Scenario* 2: *Span retraction above flutter speed*
The span morphing Goland wing is set at 1° angle of attack and the airspeed is set at 5 m/s above the flutter speed with 25% span extension. Initially, the wing starts diverging in pitch and plunge until at $t = 1$ s, where the n is retracted by 25%. Two actuation speeds are considered (1.5240 m/s and 15.240 m/s).

It is evident from Fig. 8 that span morphing can suppress flutter allowing the aircraft to operate over a wide range of airspeeds. Figure 8 also shows that the

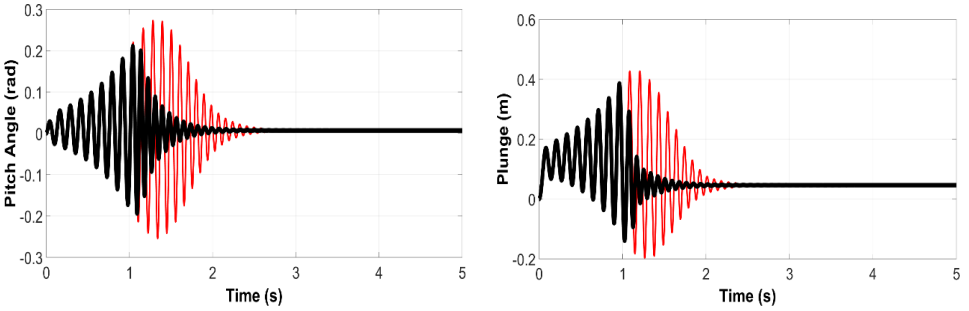

(a) Wingtip pitch angle (b) Wingtip plunge

Fig. 8. (Color online) Goland wing at 5 m/s above flutter speed and 1° AOA. At $t = 1$ s, the semi-span is retracted by 25%. Two retraction speeds are considered (red thin curve for 1.5240 m/s and black thick curve for 15.240 m/s).

wingtip's oscillations damp out faster for higher span retraction rates. Span morphing is able to significantly shift the stability of the wing. It should be noted that the choice of the actuation speeds in both scenarios is done manually without the use of a feedback control system to determine optimum retraction speeds.

6. Conclusion

This paper presented a linear aeroelastic model to study the behavior of telescopic span morphing wings in time domain. The wing was modeled as a stepped, three segment, Euler–Bernoulli beam. Rayleigh–Ritz energy method was used to derive the generalized equations of motion. Theodorsen's unsteady aerodynamic theory was used for aerodynamic predictions. A representative Padé approximation for the Theodorsen's transfer function was utilized to model the aerodynamics in state-space form, allowing time-domain simulation and analysis. The effect of the mechanical, geometric, and inertial properties of the overlapping segment and the extending segment on the aeroelastic behavior of the wing was assessed. The span extension segment (Segment 3) has significant effects on the aeroelastic behavior of the wing; however as its chord, bending rigidity, and torsional rigidity reduce, its effect on flutter significantly diminishes. In contrast, the overlapping region has higher effect on flutter speed at low span extensions, and the sensitivity of flutter to the properties of the overlapping region reduces as the wingspan increases. The effect of span morphing on the flutter mode is assessed for rectangular span morphing wing. It was found that mode 2 (first torsion) is the first to go unstable. Finally, the feasibility of utilizing span morphing as a flutter suppression device was assessed. It was found out that span morphing can act as a flutter suppression device especially if high actuation/retraction rates are used to prevent large amplitudes oscillation.

Appendix A. Bending Shape Functions

The bending shape functions for the ith bending mode for wing Segments 1, 2, and 3 can be expressed as:

$$\begin{aligned} h_{1_i}(y_1) &= A_1 \sin(b_{1_i} y_1) + B_1 \cos(b_{1_i} y_1) + C_1 \sinh(b_{1_i} y_1) + D_1 \cosh(b_{1_i} y_1), \\ h_{2_i}(y_2) &= A_2 \sin(b_{2_i} y_2) + B_2 \cos(b_{2_i} y_2) + C_2 \sinh(b_{2_i} y_2) + D_2 \cosh(b_{2_i} y_2), \\ h_{3_i}(y_3) &= A_3 \sin(b_{3_i} y_3) + B_3 \cos(b_{2_i} y_2) + C_3 \sinh(b_{3_i} y_3) + D_3 \cosh(b_{3_i} y_3). \end{aligned} \tag{A.1}$$

These shape functions can be rearranged as:

$$\begin{aligned} h_{1_i}(y_1) &= f_{1_i}(y_1)\Delta_1, \\ h_{2_i}(y_2) &= f_{2_i}(y_2)\Delta_2, \\ h_{3_i}(y_3) &= f_{3_i}(y_3)\Delta_3, \end{aligned} \tag{A.2}$$

where

$$\begin{aligned} f_{1_i}(y_1) &= [\sin(b_{1_i}y_1), \cos(b_{1_i}y_1), \sinh(b_{1_i}y_1), \cosh(b_{1_i}y_1)] \\ f_{2_i}(y_2) &= [\sin(b_{2_i}y_2), \cos(b_{2_i}y_2), \sinh(b_{2_i}y_2), \cosh(b_{2_i}y_2)] \\ f_{3_i}(y_3) &= [\sin(b_{3_i}y_3), \cos(b_{3_i}y_3), \sinh(b_{3_i}y_3), \cosh(b_{3_i}y_3)] \end{aligned} \tag{A.3}$$

and

$$\begin{aligned} \Delta_1 &= [A_1, B_1, C_1, D_1]^T, \\ \Delta_2 &= [A_2, B_2, C_2, D_2]^T, \\ \Delta_3 &= [A_3, B_3, C_3, D_3]^T. \end{aligned} \tag{A.4}$$

The constants b_{2_i} and b_{3_i} for the ith bending mode can be expressed as:

$$b_{2_i} = b_{1_i}\left(\frac{(EI)_1 m_2'}{(EI)_2 m_1'}\right)^{1/4} \tag{A.5}$$

and

$$b_{3_i} = b_{1_i}\left(\frac{(EI)_1 m_3'}{(EI)_3 m_1'}\right)^{1/4}. \tag{A.6}$$

The root, continuity, and tip boundary conditions can be rearranged in the matrix format such as

$$\begin{bmatrix} \text{Root conditions} \\ \text{Continuity conditions} \\ \text{Tip conditions} \end{bmatrix} \begin{bmatrix} \Delta_1 \\ \Delta_2 \\ \Delta_3 \end{bmatrix} = 0. \tag{A.7}$$

The dimension of the conditions matrix is n-by-n where n is equal to 4 multiplied by the number of wing's segments. To obtain the nontrivial solution (Eq. (A.7)), the determinate of the matrix is set to zero and the value of b_{1_i} is obtained numerically. Each time the determinate of the matrix becomes zero provides a new value for b_{1_i} corresponding to a vibration mode. The clamping condition at the wing root allows simplifying the first shape function to

$$h_{1_i}(y_1) = \bar{f}_{1_i}(y_1)\bar{\Delta}_1 = A_1(\sin(b_{1_i}y_1) - \sinh(b_{1_i}y_1)) + B_1(\cos(b_{1_i}y_1) - \cosh(b_{1_i}y_1)), \tag{A.8}$$

where

$$\bar{\Delta}_1 = [A_1, B_1]^T. \tag{A.9}$$

The matrices S_1, S_2, and S_3 expressed in Table A.1, represent the continuity boundary conditions for each wing segment at its ends.

The bending shape function of Segment 2 can be expressed as:

$$h_{2_i}(y_2) = f_{2_i}(y_2)[S_2(0)]^{-1}[S_1(l_1)]\bar{\Delta}_1. \tag{A.10}$$

Table A.1. Continuity boundary conditions across the wing's segments.

$S_1(l_1) = \begin{bmatrix} \bar{f}_{1_i}(l_1) \\ \bar{f}'_{1_i}(l_1) \\ (EI)_1 \bar{f}''_{1_i}(l_1) \\ (EI)_1 \bar{f}'''_{1_i}(l_1) \end{bmatrix}$	$S_2(0) = \begin{bmatrix} f_{2_i}(0) \\ f'_{2_i}(0) \\ (EI)_2 f''_{2_i}(0) \\ (EI)_2 f'''_{2_i}(0) \end{bmatrix}$
$S_2(l_2) = \begin{bmatrix} f_{2_i}(l_2) \\ f'_{2_i}(l_2) \\ (EI)_2 f''_{2_i}(l_2) \\ (EI)_2 f'''_{2_i}(l_2) \end{bmatrix}$	$S_3(0) = \begin{bmatrix} f_{3_i}(0) \\ f'_{3_i}(0) \\ (EI)_3 f''_{3_i}(0) \\ (EI)_3 f'''_{3_i}(0) \end{bmatrix}$

This can be rearranged further such as

$$h_{2_i}(y_2) = f_{2_i}(y_2) R_2 \bar{\Delta}_1 + f_{2_i}(y_2) J_2 \bar{\Delta}_1 \tag{A.11}$$

and therefore

$$[R_2, J_2] = [S_2(0)]^{-1} [S_1(l_1)]. \tag{A.12}$$

Similarly, the bending shape function of Segment 3 can be expressed as

$$h_{3_i}(y_3) = f_{3_i}(y_3) [S_3(0)]^{-1} [S_2(l_2)] [S_2(0)]^{-1} [S_1(l_1)] \bar{\Delta}_1, \tag{A.13}$$

where

$$[R_3, J_3] = [S_3(0)]^{-1} [S_2(l_2)] [S_2(0)]^{-1} [S_1(l_1)] \tag{A.14}$$

and therefore

$$h_{3_i}(y_3) = f_{3_i}(y_3) R_3 \bar{\Delta}_1 + f_{3_i}(y_3) J_3 \bar{\Delta}_1. \tag{A.15}$$

The free boundary condition (no bending moment and no shear force) at the tip of Segment 3 can be represented as

$$\begin{aligned} h''_{3_i}(l_3) &= f''_{3_i}(l_3) R_3 \bar{\Delta}_1 + f''_{3_i}(l_3) J_3 \bar{\Delta}_1 = 0, \\ h'''_{3_i}(l_3) &= f'''_{3_i}(l_3) R_3 \bar{\Delta}_1 + f'''_{3_i}(l_3) J_3 \bar{\Delta}_1 = 0. \end{aligned} \tag{A.16}$$

The tip boundary condition can be rearranged as:

$$\begin{bmatrix} f''_{3_i}(l_3) R_3 & f''_{3_i}(l_3) J_3 \\ f'''_{3_i}(l_3) R_3 & f'''_{3_i}(l_3) J_3 \end{bmatrix} \begin{bmatrix} A_1 \\ B_1 \end{bmatrix} = 0. \tag{A.17}$$

This allows expressing the shape functions as follows.

$$\begin{aligned} h_{1_i}(y_1) &= A_1[\sin(b_{1_i}y_1) - \sinh(b_{1_i}y_1)] - \frac{f''_{2_i}(l_2)R_2}{f''_{2_i}(l_2)J_2}[\cos(b_{1_i}y_1) - \cosh(b_{1_i}y_1)], \\ h_{2_i}(y_2) &= A_1\left[f_{2_i}(y_2)R_2 - J_2\frac{f''_{2_i}(l_2)R_2}{f''_{2_i}(l_2)J_2}f_{2_i}(y_2)\right], \\ h_{3_i}(y_3) &= A_1\left[f_{3_i}(y_3)R_3 - J_3\frac{f''_{2_i}(l_2)R_2}{f''_{2_i}(l_2)J_2}f_{3_i}(y_3)\right]. \end{aligned} \tag{A.18}$$

The value of A_1 can be obtained through normalization such that the shape function is unity at the wingtip. The natural frequency of the ith bending mode can be expressed as:

$$\omega_{b_i} = b_{1_i}^2\sqrt{\frac{(EI)_1}{m'_1}}. \tag{A.19}$$

Appendix B. Torsion Shape Function

The torsion shape functions for the ith vibration mode for wing Segments 1, 2, and 3 can be expressed as:

$$\begin{aligned} \phi_{1_i}(y_1) &= a_1\sin(k_{1_i}y_1) + b_1\cos(k_{1_i}y_1), \\ \phi_{2_i}(y_2) &= a_2\sin(k_{2_i}y_2) + b_2\cos(k_{2_i}y_2), \\ \phi_{3_i}(y_3) &= a_3\sin(k_{3_i}y_3) + b_3\cos(k_{3_i}y_3). \end{aligned} \tag{B.1}$$

These shape functions can be rearranged as:

$$\begin{aligned} \phi_{1_i}(y_1) &= \eta_{1_i}(y_1)\lambda_1, \\ \phi_{2_i}(y_2) &= \eta_{2_i}(y_2)\lambda_2, \\ \phi_{3_i}(y_3) &= \eta_{3_i}(y_3)\lambda_3, \end{aligned} \tag{B.2}$$

where

$$\begin{aligned} \eta_{1_i}(y_1) &= [\sin(k_{1_i}y_1), \cos(k_{1_i}y_1)], \\ \eta_{2_i}(y_2) &= [\sin(k_{2_i}y_2), \cos(k_{2_i}y_2)], \\ \eta_{3_i}(y_3) &= [\sin(k_{3_i}y_3), \cos(k_{3_i}y_3)], \end{aligned} \tag{B.3}$$

and

$$\begin{aligned} \lambda_1 &= [a_1, b_1]^T, \\ \lambda_2 &= [a_2, b_2]^T, \\ \lambda_3 &= [a_3, b_3]^T. \end{aligned} \tag{B.4}$$

The constants k_{2_i} and k_{3_i} for the ith torsional vibration mode can be expressed as

$$k_{2_i} = k_{1_i}\left(\frac{(GJ)_1 I'_{\text{ea}_2}}{(GJ)_2 I'_{\text{ea}_1}}\right)^{1/2} \tag{B.5}$$

and

$$k_{3_i} = k_{1_i}\left(\frac{(GJ)_1 I'_{\text{ea}_3}}{(GJ)_3 I'_{\text{ea}_1}}\right)^{1/2}. \tag{B.6}$$

The dimension of the coefficients matrix is m-by-m where m is equal to 2 multiplied by the number of wing segments. The coefficient matrix can be expressed as

$$\begin{bmatrix} \text{Roots conditions} \\ \text{Continuity conditions} \\ \text{Tip conditions} \end{bmatrix} \begin{bmatrix} \lambda_1 \\ \lambda_2 \\ \lambda_3 \end{bmatrix} = 0. \tag{B.7}$$

To obtain the nontrivial solution of the above equations, the determinate of the left-hand side matrix must be set to zero. This is solved iteratively to find the values of k_{1_i} that make the determinate of the matrix zero. Each time the determinate becomes zero represents a new vibration mode (1st, 2nd, etc.). The clamping conditions at the root result in $b_1 = 0$. Using the continuity boundary conditions, the coefficients a_2, a_3, b_2, and b_3 can be expressed as:

$$a_2 = a_1 \frac{k_{1_i}(GJ)_1}{k_{2_i}(GJ)_2}\cos(k_{1_i} l_1), \tag{B.8}$$

$$b_2 = a_1 \sin(k_{1_i} l_1), \tag{B.9}$$

$$a_3 = \frac{k_{2_i}(GJ)_2}{k_{3_i}(GJ)_3}[a_2 \cos(k_{2_i} l_2) - b_2 \sin(k_{2_i} l_2)], \tag{B.10}$$

and

$$b_3 = a_2 \sin(k_{2_i} l_2) + b_2 \cos(k_{2_i} l_2). \tag{B.11}$$

It should be noted that a_2, a_3, b_2, and b_3 depend on a_1. The value of a_1 can be obtained through normalization such that the shape function is unity at the tip. The natural frequency of the ith torsion mode can be expressed as:

$$\omega_{t_i} = k_{1_i}\sqrt{\frac{(GJ)_1}{I'_{\text{ea}_1}}}. \tag{B.12}$$

References

1. S. Barbarino, O. Bilgen, R. M. Ajaj, M. I. Friswell and D. J. Inman, A review of morphing aircraft, *J. Intell. Mater. Syst. Struct.* **22**(9) (2011) 823–877.
2. R. M. Ajaj, C. S. Beaverstock and M. I. Friswell, Morphing aircraft: The need for a new design philosophy, *Aerosp. Sci. Technol.* **49** (2016) 154–166.

3. R. M. Ajaj, M. I. Friswell, E. I. Saavedra Flores, A. J. Keane, A. T. Isikveren, G. Allegri and S. Adhikari, An integrated conceptual design study using span morphing technology, *J. Intell. Mater. Syst. Struct.* **25**(8) (2014) 989–1008. doi: 10.1177/1045389X13502869
4. R. M. Ajaj, M. I. Friswell, E. I. Saavedra Flores, O. Little and A. T. Isikveren, Span morphing: A conceptual design study, in *20th AIAA/ASME/AHS Adaptive Structures Conf.*, 23–26th April 2012, Honolulu, Hawaii, USA, AIAA-2012-1510.
5. T. A. Weisshaar, Morphing aircraft technology — New shapes for aircraft design, RTO-MP-AVT-141, Neuilly-sur-Seine, France (2006).
6. J. Blondeau and D. Pines, Design and testing of a pneumatic telescopic wing for unmanned aerial vehicles, *AIAA J. Aircr.* **44**(4) (2007) 1088–1099.
7. J. S. Bae, T. M. Seigler and D. J. Inman, Aerodynamic and aeroelastic characteristics of a variable-span morphing wing, *J. Aircr.* **42**(2) (2005) 528–534.
8. R. M. Ajaj and G. Jankee, The transformer aircraft: A multi-mission unmanned aerial vehicle capable of symmetric and asymmetric span morphing, *Aerosp. Sci. Technol.* **76** (2018) 512–522.
9. P. Santos, J. Sousa and P. Gamboa, Variable-span wing development for improved flight performance, *J. Intell. Mater. Syst. Struct.* **28**(8) (2017) 961–978.
10. J. Mestrinho, J. Felício, P. Santos and P. Gamboa, Design optimization of a variable-span morphing wing, in *2nd International Conf. Engineering Optimization*, 6–9 September 2010, Lisbon, Portugal.
11. J. Felício, P. Santos, P. Gamboa and M. Silvestre, Evaluation of a variable-span morphing wing for a small UAV, in *52nd AIAA/ASME/ASCE/AHS/ASC Structures, Structural Dynamics and Materials Conf. Structures, Structural Dynamics, and Materials* (2011), Colorado, USA.
12. R. M. Ajaj and M. I. Friswell, Aeroelasticity of compliant span morphing wings, *Smart Mater. Struct.* **27**(10) (2018). http://iopscience.iop.org/article/10.1088/1361-665X/aad219.
13. R. Huang and Z. Qiu, Transient aeroelastic responses and flutter analysis of a variable-span wing during the morphing process, *Chin. J. Aeronaut.* **26**(6) (2013) 1430–1438.
14. W. Li and D. Jin, Flutter suppression and stability analysis for a variable-span wing via morphing technology, *J. Sound Vib.* **412** (2018) 410–423. https://doi.org/10.1016/j.jsv.2017.10.009
15. P. Gamboa, J. Silva and P. Santos, Flutter analysis of a composite variable-span wing, in *4th Int. Conf. Integrity, Reliability and Failure*, Funchal/Madeira, 23–27 June (2013).
16. M. Goland, The flutter of a uniform cantilever wing, *J. Appl. Mech.* **12**(4) (1945) A-197–A-208.
17. B. Raghavan and M. J. Patil, Flight dynamics of high aspect-ratio flying wings: Effect of large trim deformation, *J. Aircr.* **46**(5) (2009) 1808–1812.
18. T. Theodorsen, General theory of aerodynamic instability and the mechanism of flutter, Technical Report No. 496, NACA (1935).
19. J. B. Duan and Z. Y. Zhang, Aeroelastic stability analysis of aircraft wings with high aspect ratios by transfer function method, *Int. J. Struct. Stab. Dyn.* **18**(12) (2018) 1850150.
20. S. L. Brunton and C. W. Rowley, Low-dimensional state-space representations for classical unsteady aerodynamic models, in *49th AIAA Aerospace Sciences Meeting Including the New Horizons Forum and Aerospace Exposition*, Orlando, Florida (2011), AIAA-2011-476.
21. R. D. Breuker, M. Abdallah, A. Milanese and P. Marzocca, Optimal control of aeroelastic systems using synthetic jet actuators, in *49th AIAA/ASME/ASCE/AHS/ASC Structures, Structural Dynamics, and Materials Conf.*, IL, USA (2008), AIAA-2008-1726.

22. M. J. Patil, D. H. Hodges and C. E. S. Cesnik, Nonlinear aeroelasticity and flight dynamics of high-altitude, long-endurance aircraft, *J. Aircr.* **38**(1) (2001) 88–94.
23. M. J. Patil, D. H. Hodges and C. E. S. Cesnik, Nonlinear aeroelastic analysis of complete aircraft in subsonic flow, *J. Aircr.* **37**(5) (2000) 753–760. https://doi.org/10.2514/2.2685
24. M. J. Patil, Aeroelastic tailoring of composite box beams, in *Proc. 35th Aerospace Sciences Meeting and Exhibit*, Reno, Nevada (1997).